Cancer Biol Med 2025. doi: 10.20892/j.issn.2095-3941.2024.0483

ORIGINAL ARTICLE

IL-33/ST2 signalling promotes tumor growth by regulating polarization of alternatively activated macrophages

Liping Liu, Haoge Luo, Yingdong Xie, Ying Wang, Shiying Ren, Haiyang Sun, Dong Li

Key Laboratory of Pathobiology, Ministry of Education, Department of Immunology, College of Basic Medical Sciences, Jilin University, Changchun 130021, China

ABSTRACT

Objective: Suppression of tumorigenicity 2 (ST2), the receptor for interleukin (IL)-33, has a critical role in tumor growth, angiogenesis, metastasis, and immune modulation. The IL-33/ST2 pathway is known to influence the polarization and function of macrophages, which is integral to modulating the tumor microenvironment. However, the precise role of IL-33/ST2 in tumors, particularly non-small cell lung cancer (NSCLC), has not been established.

Methods: ST2 expression in NSCLC was analysed using a murine model and patient specimens. The effect of the IL-33/ST2 axis on macrophage polarization in NSCLC was determined.

Results: Elevated *ST2* expression was correlated with aggressive tumor growth. Specifically, *ST2* expression on macrophages was associated with lung cancer progression and the absence of *ST2* on macrophages was associated with diminished tumor growth. IL-33 promoted polarization of alternatively activated macrophages in an ST2-dependent manner that was mediated *via* the PI3K/Akt signalling pathway. Moreover, IL-33 inhibited T-cell function by inducing the secretion of transforming growth factor β from alternatively activated macrophages.

Conclusions: Macrophages expressing ST2 can serve as promising therapeutic targets for NSCLC immunotherapy, highlighting the IL-33/ST2 axis as a potential target for future antitumor strategies.

KEYWORDS IL-33; ST2; macrophage polarization; non-small cell lung cancer; tumor microenvironment

Introduction

Lung cancer accounts for approximately 20% of all cancer-related deaths owing to high morbidity and mortality rates[1]. Among primary lung cancers, non-small cell lung cancer (NSCLC) constitutes approximately 85% of cases[2]. Treatments for NSCLC are still limited. Current immunotherapies, such as immune checkpoint inhibitors and CAR-T cells, are far from ideal and have been reported to trigger immune-related adverse events[3-5]. One critical reason for the limited success of many effective lung cancer therapies is the tumor microenvironment (TME), which directly influences treatment resistance[6,7]. Therefore, research is required to identify additional strategies to modulate the TME.

Suppression of tumorigenicity 2 (ST2), encoded by the interleukin-1 receptor-like 1 gene (*IL1RL1*), functions as an interleukin (IL)-33 receptor and was originally considered a stable surface marker of Th2 cells[8,9]. ST2L and sST2 are two major isoforms of ST2. ST2L binds to IL-33 and triggers type 2 immunity, while sST2 negatively regulates IL-33/ST2 signalling by serving as a decoy receptor and sequestering IL-33 to block its interaction with ST2L[10,11]. Recent evidence showed that ST2L and sST2 influence the TME and progression of many cancers[12-15]. However, the role of IL-33/ST2 axis in lung cancer is controversial.

Tumor-associated macrophages (TAMs) exhibit an alternatively activated macrophage (AAM)-like gene expression profile that exerts anti-inflammatory and pro-tumorigenic activities, which constitute the most dominant immune cell population in the TME[16-18]. Reprogramming tumor-infiltrating macrophages to a classically activated macrophage (CAM)-like phenotype has proven to be beneficial for tumor treatment[19,20]. CAM-like polarized macrophages promote

Correspondence to: Dong Li
E-mail: lidong1@jlu.edu.cn
ORCID ID: https://orcid.org/0000-0002-2508-3282
Received October 26, 2024; accepted February 20, 2025;
published online March 27, 2025.
Available at www.cancerbiomed.org
©2025 The Authors. Creative Commons Attribution-NonCommercial 4.0 International License

type-I immune responses against bacterial and viral infections, as well as tumor cells[18,21]. Our previous studies showed that activation of ST2 *via* its ligand (IL-33) polarizes macrophages to an AAM-like phenotype, whereas blockage of the IL-33/ST2 pathway leads to CAM-like polarization[22,23]. However, the exact role of IL-33/ST2 in promoting AAM polarization in NSCLC is unclear.

In the current study the effect of IL-33 in the TME on NSCLC progression was determined. Higher ST2 expression led to more aggressive tumor growth. *St2* knockout macrophages had beneficial effects in a murine NSCLC model. IL-33 created an immunosuppressive environment by promoting the polarization of AAMs in an ST2-dependent manner through activation of the PI3K/Akt signalling pathway. Additionally, IL-33 inhibited T-cell function *via* induction of TGF-β from AAMs. The IL-33/ST2 axis was shown to promote NSCLC and immunosuppression, thereby providing a potential therapeutic target for patients with NSCLC.

Materials and methods

Cell culture

Mouse lung carcinoma [Lewis] (Guangzhou Cellcook Biotech Co. Ltd. Guangzhou, China), L929, and 293T cells were cultured in Dulbecco's Modified Eagle's Medium [DMEM] (Sartorius CellGenix GmbH, Freiburg, Germany) supplemented with 10% foetal bovine serum [FBS] (Sartorius) and 1% penicillin/streptomycin (Solarbio, Beijing, China). Bone marrow cells were removed from mice (6–8 weeks old) and cultured for 7 days in DMEM supplemented with 10% FBS, 1% penicillin/streptomycin, and 30% conditioned medium from the L929 cells to differentiate into bone marrow-derived macrophages (BMDMs). All cells were cultured in an incubator (Thermo Fisher Scientific, Waltham, MA, USA) at 37°C under 5% CO_2. All cell lines were purchased from Guangzhou Cellcook with confirmation of genotypic authentication or acquired from our laboratory.

Animals and tumor models

Il33 transgene ($Il33^{Tg}$), *Il33*-deficient ($Il33^{-/-}$), and *Il1rl1*-deficient ($St2^{-/-}$) mice were purchased from Cyagen Biosciences, Inc. (Suzhou, China). All animals were housed under specific pathogen-free (SPF) conditions in temperature-controlled, air-conditioned facilities with unlimited access to food and water. Wide-type (WT) mice were obtained from the same litter. Lewis cells (1×10^6) were injected subcutaneously into the right dorsum of mice to create a mouse tumor model. Tumor volume was estimated using the following formula: tumor volume (mm^3) = [length (mm) × short $(mm)^2$]/2. Mouse models of carcinoma *in situ* were established, as previously described[24]. Mice were anesthetized using an intraperitoneal injection of Avertin (200 μL [20 mg/mL] 2,2,2-tribromoethanol; Sigma-Aldrich, St. Louis, MO, USA). The lungs were then exposed surgically by making an incision (0.5 cm long) in the left chest and 2×10^5 Lewis cells resuspended in 20 μL of Corning Matrigel (Corning, NY, USA) were injected into the lower left lung using a plastic, 1-mL insulin needle. The surgical wounds were closed with sutures. The mice were randomly assigned to 2 different groups 7 d later and BMDMs (1×10^6 cells/mouse) derived from WT and $St2^{-/-}$ mice were injected into the tail vein with repeated injections on day 10. The mice were sacrificed on day 14. All experiments were performed in accordance with the National Guidelines for Experimental Animal Welfare and were approved by the Animal Welfare and Research Ethics Committee of Jilin University (Approval no. 2022:95) prior to initiation of the study.

Human lung cancer sample and spatial transcriptomics

Surgically resected lung cancer tissues were obtained from a 61-year-old male with moderately differentiated invasive adenocarcinoma and a 71-year-old male with moderately differentiated invasive adenocarcinoma and immediately submerged in cold phosphate-buffered saline [PBS] (Bioss, Beijing, China) and cut into approximately 5 mm-thick sections. The bulk tissues were placed in an OCT-filled mould (SAKURA, Tokyo, Japan) and snap-frozen on dry ice. Spatial transcriptome sequencing based on the Visium Technology Platform from 10 × Genomics was performed by Shanghai Majorbio Bio-pharm Technology Co., Ltd. (Shanghai, China). Written informed consent was obtained from all participants. This study was approved by the Ethics Committee of the First Hospital of Jilin University (Approval no. 2024:8).

Survival and correlation analyses

The online Kaplan–Meier plotter tool (https://kmplot.com/analysis/) was used for survival analysis. GEPIA 2 (http://gepia2.

cancer-pku.cn/#index) was used for correlation analysis of *ST2* expression with *CD163* in the lung adenocarcinoma database.

Immunohistochemistry

Tumor tissues from mice were formalin-fixed and paraffin-embedded on slides and the paraffin-embedded tissues were de-paraffinised and rehydrated. Antigens were retrieved in a heated citrate buffer (Beyotime, Shanghai, China) for 1 h and incubated with a 3% bovine serum albumin (BSA, Sigma-Aldrich) blocking solution at room temperature for 30 min. The slides were then incubated with anti-CD31 antibody (Cell Signaling Technology, Danvers, MA, USA) overnight at 4°C. The slides were further incubated with the immunohistochemistry (IHC) detection reagent and visualised using a secondary antibody and DAB peroxidase substrate (Fuzhou Maixin Biotech. Co., Ltd, Fuzhou, China).

Immunofluorescence

Tumor tissue sections were incubated with primary antibodies (anti-ST2; R&D Systems, Minneapolis, MN, USA) and (anti-CD206; Cell Signaling Technology) at 4°C overnight, followed by incubation with the corresponding antibodies for 1 h at room temperature. Nuclei were stained with 4′,6-diamidino-2-phenylindole [DAPI] (Beyotime) for 5 min. The slides were mounted on coverslips and imaged under a microscope (Olympus, Tokyo, Japan).

Cell proliferation

BMDMs from WT and $St2^{-/-}$ mice were cultured in 96-well plates for 48 h to study cellular proliferation. Lewis cells were co-cultured with BMDM-Ctrl, BMDM-*flIl33*, or BMDM-*cIl33* cells for 48 h. The Cell Counting Kit-8 [CCK-8] (Bioss) was used to detect cell proliferation based on absorbance values following the manufacturer's protocol.

Invasion assay

Cellular invasion was measured using Transwell inserts containing 8-μm membrane filters (LABSELECT, Jinan, China). Lewis cells (2×10^4) were seeded in serum-free medium in the upper chamber of a Transwell insert coated with Matrigel (Corning). BMDM-Ctrl, BMDM-*flIl33*, and BMDM-*cIl33* cells (1×10^5) in fresh medium containing 10% FBS were seeded in the lower Transwell chamber. After incubation for 24 h, cells on the upper surface were washed with PBS, fixed with 4% paraformaldehyde for 15 min, and stained with 0.1% crystal violet for 15 min. Invasive cells were counted under a microscope.

Lentiviral packaging and overexpression assay

Lentiviral production and transduction were performed using a lentiviral vector containing a lentiviral packaging mix. The following mouse lentivirus packaging plasmids were purchased from HanBio Biotechnology Co., Ltd. (Shanghai, China): control, full-length *Il33* (*flIl33*, 1–266 amino acids); *Il33* C-terminal domain (*cIl33*, 109–266 amino acids); pMD2G plasmids; and psPAX2 plasmids First, the plasmids were extracted (TransGen Biotech, Beijing, China) and transfected into 293T cells using a transfection reagent (Yeasen, Shanghai, China) for 48 h. The supernatant was collected and centrifuged in ultrafiltration tubes (Merck, Darmstadt, Germany) to obtain the lentivirus. The lentivirus was transfected into Lewis cells using polybrene (Yeasen) and puromycin (Sigma-Aldrich) was added 72 h after transfection to screen the cells. After 1 week of screening, stable monoclonal cells were obtained, including Lewis-Ctrl, Lewis-*flIl33*, and Lewis-*cIl33*. To obtain BMDMs expressing *flIl33* and *cIl33*, the lentivirus was transfected into BMDMs, BMDM-Ctrl, BMDM-*flIl33*, and BMDM-*cIl33* cells were obtained after transfection for 72 h.

Flow cytometry analysis

Fresh tumor tissues were cut into small pieces. The tissues were dissociated using a grinder and centrifuged at 400×*g* for 5 min. The erythrocytes were lysed (Solarbio) and the cell suspension was incubated with antibodies. The cultured cells were then processed. Briefly, 100 μL of the cell suspension was incubated for 10 min with FcR blocking reagent (Miltenyi Biotec, Bergisch Gladbach, Germany). The cells were washed with PBS to remove the unbound FcR blocking reagent. For surface staining, APC anti-mouse CD45 antibody (BioLegend, San Diego, CA, USA), PerCP anti-mouse F4/80 antibody (BD Biosciences, San Jose, CA, USA.), PE anti-mouse CD206 antibody (BD Biosciences), FITC anti-mouse CD11c antibody (BD Biosciences), PE anti-mouse NK1.1 antibody (BD Biosciences), PE anti-mouse B220 antibody (BD Biosciences), PE anti-mouse CD3 antibody (eBioscience, USA), FITC anti-mouse CD4 antibody (eBioscience, San Diego, CA, USA),

PerCP-Cy5.5 anti-mouse CD8 antibody (eBioscience), APC anti-mouse CD279 (PD-1) antibody (BioLegend), and PerCP anti-mouse CTLA4 antibody (BioLegend) were added as appropriate, incubated at 4°C for 30 min, and washed with the FACS buffer (1% FBS in PBS). To stain intracellular molecules, cells were fixed with 4% paraformaldehyde for 50 min, washed twice with 0.1% saponin-PBS for permeabilisation, stained with the PE anti-mouse IFNγ antibody (eBioscience), PE anti-mouse perforin antibody (eBioscience), PE anti-mouse Foxp3 antibody (Biolegend) as appropriate for 45 min, washed with FACS buffer. All samples were analysed using a flow cytometer (Guava Technologies, Hayward, CA, USA) and analysed using FlowJo v10 (FlowJo, LLC, Ashland, OR, USA).

Macrophage phagocytosis

BMDMs from WT and *St2*$^{-/-}$ mice were cultured in 6-well plates. Lewis cell debris with GFP fluorescence was added to the culture supernatant and incubated for 24 h. The BMDMs were collected, labelled with F480 antibody, and the percentage of F480-positive cells containing GFP was detected using flow cytometry.

Enzyme-linked immunosorbent assay (ELISA)

The cytokine concentration in the culture media from co-culture experiments and tumor tissues was quantitatively determined using an ELISA following the manufacturer's instructions, including TGF-β (Solarbio) and IL-33 (R&D Systems). The absorbance of each well was measured at 450 nm using a microplate reader (EPOCH2, BioTek, Winooski, VT, USA).

Quantitative real-time polymerase chain reaction

Total RNA was extracted using TRIzol reagent (Takara, Kusatsu, Japan) and reverse-transcribed into cDNA using a cDNA Synthesis Kit (TOLO Biotechnology, Shanghai, China). Real-time PCR was performed using an Agilent Mx3000P machine (Agilent, Santa Clara, CA, USA) with SYBR Green Master Mix (Takara). The following forward and reverse primer sequences for the test genes were used: *Gapdh* (forward, 5′-GCACCGTCAAGGCTGAGAAC-3′; reverse, 5′-GGATCTCGCTCCTGGAAGATG-3′); *Mrc1* (forward, 5′-CTCTGTTCAGCTATTGGACGCCG-3′); reverse, 5′-TGGCACTCCCAAACATAATTTGA-3′); *Tgfb* (forward, 5′-AGGCGGTGCTCGCTTTGTA-3′; reverse, 5′-CTGCTTCCCGAATGTCTGA-3′); and *Arg1* (forward, 5′-CTCCAAGCCAAAGTCCTTAGAG-3′; reverse, 5′-AGGAGCTGTCATTAGGGACA-3′). The target mRNA expression was calculated relative to the amount of GAPDH using the $2^{-\Delta\Delta Ct}$ method.

Western blot analysis

The total cellular protein was collected and lysed using RIPA (Beyotime) and protease inhibitors (Roche, Basel, Switzerland) at 4°C for 30 min, centrifuged at 10,000 × *g* for 30 min, and the supernatant was collected. The protein concentration was determined using a BCA Protein Quantification Kit (Biomed, Beijing, China). All samples were separated by sodium dodecyl sulfate-polyacrylamide gel electrophoresis (SDS-PAGE) and transferred onto polyvinylidene fluoride (PVDF) membranes (Merck). The membrane was blocked with 5% skim milk at room temperature for 2 h followed by incubation overnight at 4°C with the primary antibody against CD206 (Cell Signaling Technology), PI3K (ZenBio Science, Chengdu, China), P-PI3K (Affinity Biosciences, Changzhou, China), Akt (ZenBio Science), P-Akt (ZenBio Science), and GAPDH (Wuhan Sanying, Wuhan, China). The PVDF membranes were washed three times with Tris-buffered saline with Tween-20 [TBST] (Solarbio) for 5 min each, incubated with an HRP-conjugated secondary antibody (Bioss) for 40 min at room temperature, then washed three times with TBST. Specific bands were detected using an enhanced chemiluminescence detection reagent (Sparkjade, Jinan, China).

RNA sequencing (RNA-Seq) analysis

RNA-Seq was performed by Sangon Biotechnology (Shanghai, China). Briefly, BMDMs from WT, *Il33*^{Tg}, and *St2*$^{-/-}$ mice were stimulated with IL-4 for 48 h and total RNA was extracted using the TRIzol Reagent (Takara). RNA integrity was assessed using an Agilent Bioanalyzer 2100. Only samples with clean rRNA profiles were used in the subsequent steps. Paired-end sequencing was performed using an Illumina HighSeq 4000 instrument (Illumina, San Diego, CA, USA).

Macrophage and Lewis cell co-culture

Macrophages and Lewis cells were co-cultured using Transwell inserts containing 0.4-μm membrane filters (LABSELECT). BMDMs from WT or *St2*$^{-/-}$ mice were placed in the lower

Transwell chamber with Lewis-NC (Lewis cells). Lewis-Ctrl, Lewis-*flIl33*, and Lewis-*cIl33* cells were added to the upper Transwell chamber and incubated for 48 h. The PI3K/Akt signalling pathway was inhibited using a PI3K-IN-1 inhibitor (catalog no. HY-12068; MCE, Monmouth Junction, NJ, USA) in the co-culture system.

T cell sorting

T cells were sorted using the EasySep™ Mouse $CD8^+$ T Cell Isolation Kit and the EasySep™ Mouse $CD4^+$ T Cell Isolation Kit (STEMCELL, Vancouver, Canada) following the manufacturer's instructions. Briefly, splenocytes were resuspended in Dulbecco's phosphate-buffered saline [DPBS] (Servicebio, Wuhan, China). One millilitre of the cell suspension was placed in a sorting tube. An FcR blocker and isolation cocktail were then added to the sample and incubated for 10 min. RapidSpheres™ were added to the samples and incubated for 5 min. Subsequently, 1.3 mL of DPBS was added to give a final volume of 2.5 mL. The sorting tube was placed in a magnet apparatus for 5 min at room temperature and the supernatants containing the cells were collected and used for further experiments.

Supernatants stimulate T cells

The BMDM supernatants co-cultured with Lewis-NC, Lewis-Ctrl, Lewis-*flIl33*, and Lewis-*cIl33* were collected and used to resuspend sorted $CD4^+$ T cells and $CD8^+$ T cells, which were subsequently incubated in 96-well plates for 72 h. TGF-β was neutralised using TGF-β neutralising antibody (Biolegend). The cells were collected for subsequent experiments.

Statistical analysis

All experimental results were obtained from at least three replicates. The sample size for both the animal model and *in vitro* experiments was decided based on expected variance and standard deviations from pilot studies. The significance was set at 0.05 with a power of 0.9 following the guidelines published in *ILAR Journal*[25]. The statistical significance of differences was tested using one-way analysis of variance (ANOVA) or unpaired two-tailed *t*-tests. The results are presented as the mean ± standard deviation (SD). Analyses were performed using GraphPad Prism software (version 8.0; GraphPad Software, Boston, MA, USA). Statistical significance was set at a $P < 0.05$.

Results

ST2 expression on macrophages is associated with lung cancer

Immunofluorescence analysis was performed on mouse lung cancer samples to determine the clinical relevance of ST2 in the context of lung adenocarcinoma (LUAD). Th ST2 expression was significantly higher in tumor tissues compared to adjacent normal lung tissues (**Figure 1A**). A Kaplan–Meier plot generated from an online dataset comprised of 10 independent cohorts (a total of 1161 patients) revealed that high ST2 expression correlates with reduced survival rates in patients with LUAD (**Figure S1**)[26]. The detailed characteristics of each dataset are presented in **Table S1**. WT, $Il33^{Tg}$, $Il33^{-/-}$, and $St2^{-/-}$ mice were inoculated with Lewis lung carcinoma cells to further investigate the role of IL-33/ST2 in lung cancer. The growth of tumors was faster in $Il33^{Tg}$ mice (**Figure 1B**), while *Il33* and *St2* knockout inhibited tumor growth (**Figure 1C**). These results suggested that the IL-33/ST2 axis promotes lung cancer progression.

ST2 expression was determined in various cell types by analysing single-cell sequencing data from 49 patients with lung cancer to identify the cells in the TME with high ST2 expression[27]. *ST2* was expressed in macrophages, fibroblasts, and T cells (**Figure 1D**). Macrophage polarization has an important role in the TME. A correlation analysis was performed using data from the GEPIA2 website to determine the relevance of *ST2* and AAMs in lung adenocarcinoma[28]. Expression of *ST2* and *CD163*, which are primarily expressed in AAMs[29], was shown to be positively correlated with LAUD (**Figure 1E**). Moreover, spatial transcriptomic data from biopsy tissues of patients with LUAD showed overlapping expression of *ST2* and *CD163* in tumor tissues (**Figure 1F**). These data highlighted the potential functional role of $ST2^+$ macrophages in lung cancer.

Cell transfer of $St2^{-/-}$ BMDMs inhibit tumor growth

St2 was knocked out and the effect on macrophage function was determined *in vitro*. *St2* knockout did not affect the proliferative and phagocytic function of macrophages (**Figure 2A, B**). A mouse model of carcinoma *in situ* was constructed by inoculating the lungs of mice with Lewis cells to further determine whether *St2* knockout macrophages ($St2^{-/-}$ BMDMs)

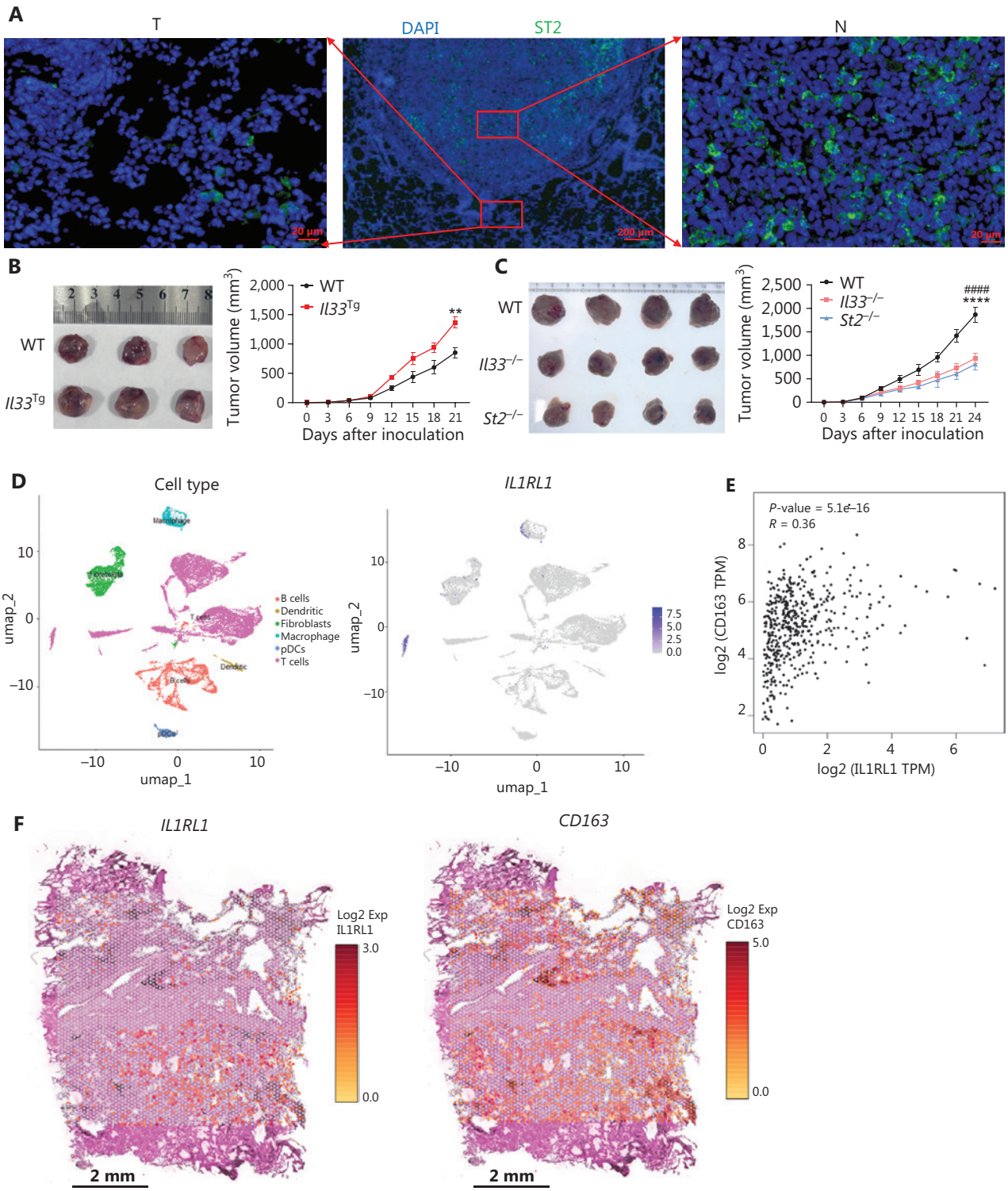


Figure 1 ST2 expression on macrophages is associated with lung cancer. (A) Representative images of ST2 expression in formalin-fixed, paraffin-embedded lung cancer tissue sections from mouse (T) and adjacent normal lung tissues (N), ST2 (green), and DAPI (blue). Scale bar, 20 μm (left and right), 200 μm (middle); (B) Tumor size (left) and the change of tumor volume (right) after Lewis cells were inoculated in WT and *Il33*^{Tg} mice (n = 3); (C) Tumor size (left) and the change of tumor volume (right) after Lewis cells were inoculated in WT, *Il33*$^{-/-}$, and *St2*$^{-/-}$ mice (n = 4), * WT *vs.* *Il33*$^{-/-}$, # WT *vs.* *St2*$^{-/-}$; (D) UMAP showing the distribution and clusters of *ST2* in patients with lung cancer using

single-cell RNA-sequencing data; (E) Correlation analysis of *ST2* and *CD163* genes using the database of patients with lung adenocarcinoma from the GEPIA2 website; (F) H&E staining and the spatial cluster distribution of *ST2* and *CD163* in tumor tissues of patients with lung adenocarcinoma. Scale bar, 2 mm. Data are shown as the mean ± SD and analysed using one-way ANOVA or an unpaired two-tailed *t*-test. $^{**}P < 0.01$, $^{****}P < 0.0001$, $^{\#\#\#\#}P < 0.0001$. ST2, suppression of tumorigenicity 2; UMAP, Uniform Manifold Approximation and Projection; H&E, haematoxylin and eosin.

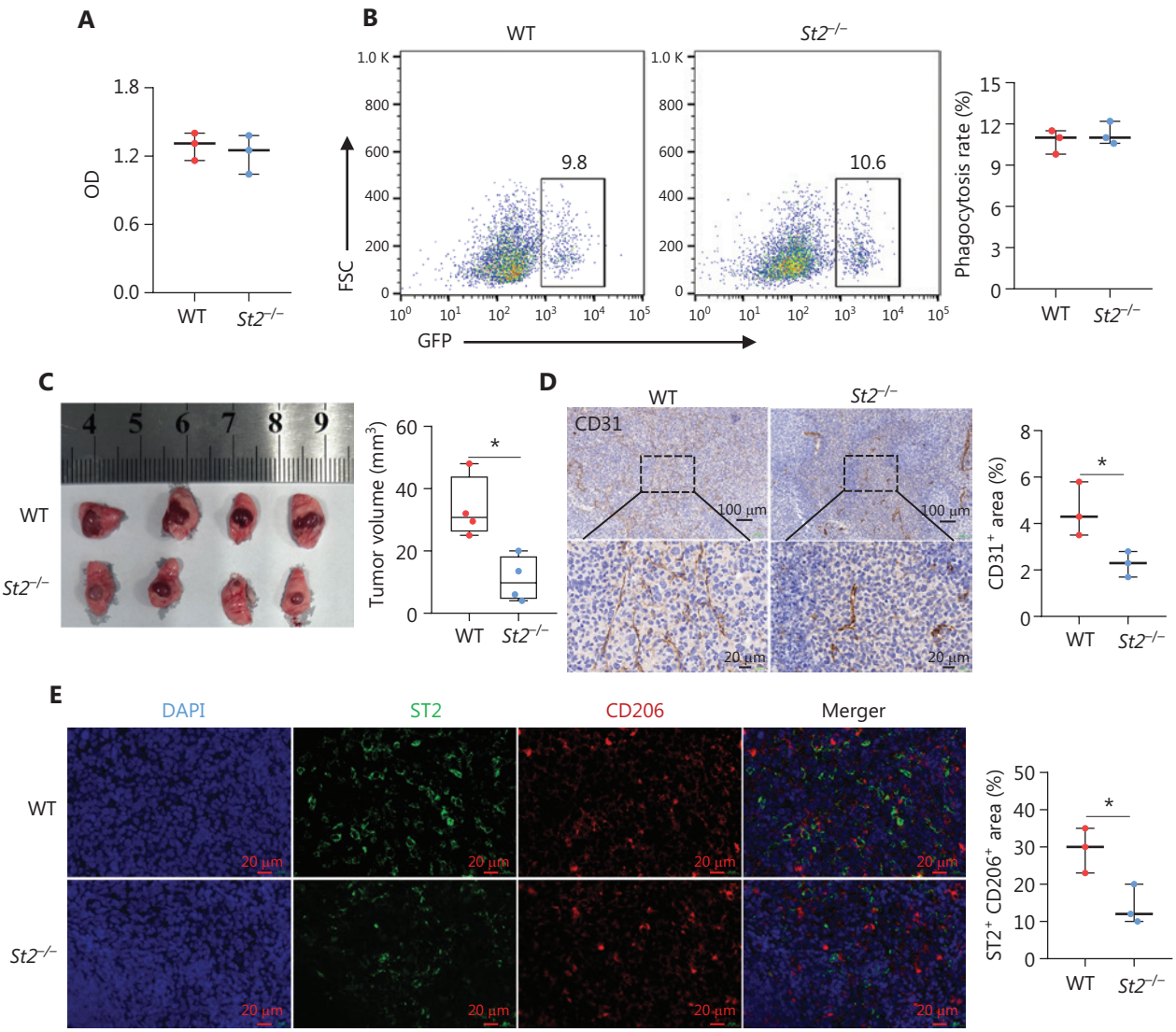


Figure 2 Cell transfer of *St2*$^{-/-}$ BMDMs inhibits tumor growth. (A) The effect of *St2* knockout on the proliferative capacity of macrophages using CCK-8; (B) The effect of *St2* knockout on the phagocytosis of macrophages using flow cytometry; (C) Tumor size (left) and tumor volume (right) after WT BMDMs and *St2*$^{-/-}$ BMDMs were administered to the carcinoma *in situ* mice *via* the tail vein (n = 4); (D) Representative IHC images (left) and quantification analysis (right) of CD31 in tumor tissue sections after WT BMDMs and *St2*$^{-/-}$ BMDMs were administered to the carcinoma *in situ* mice *via* the tail vein, scale bar, 100 μm (up), 20 μm (down); (E) Representative IF images (left) and quantification analysis (right) of ST2 and CD206 in formalin-fixed, paraffin-embedded sections of lung cancer tissue after WT BMDMs and *St2*$^{-/-}$ BMDMs were administered to the mice with carcinoma *in situ via* the tail vein. Scale bar, 20 μm. Data are shown as the mean ± SD and analysed using an unpaired two-tailed *t*-test. $^{*}P < 0.05$. ST2, suppression of tumorigenicity 2; BMDM, bone marrow-derived macrophages; CCK-8, Cell Counting Kit-8; IHC, immunohistochemistry; IF, immunofluorescence.

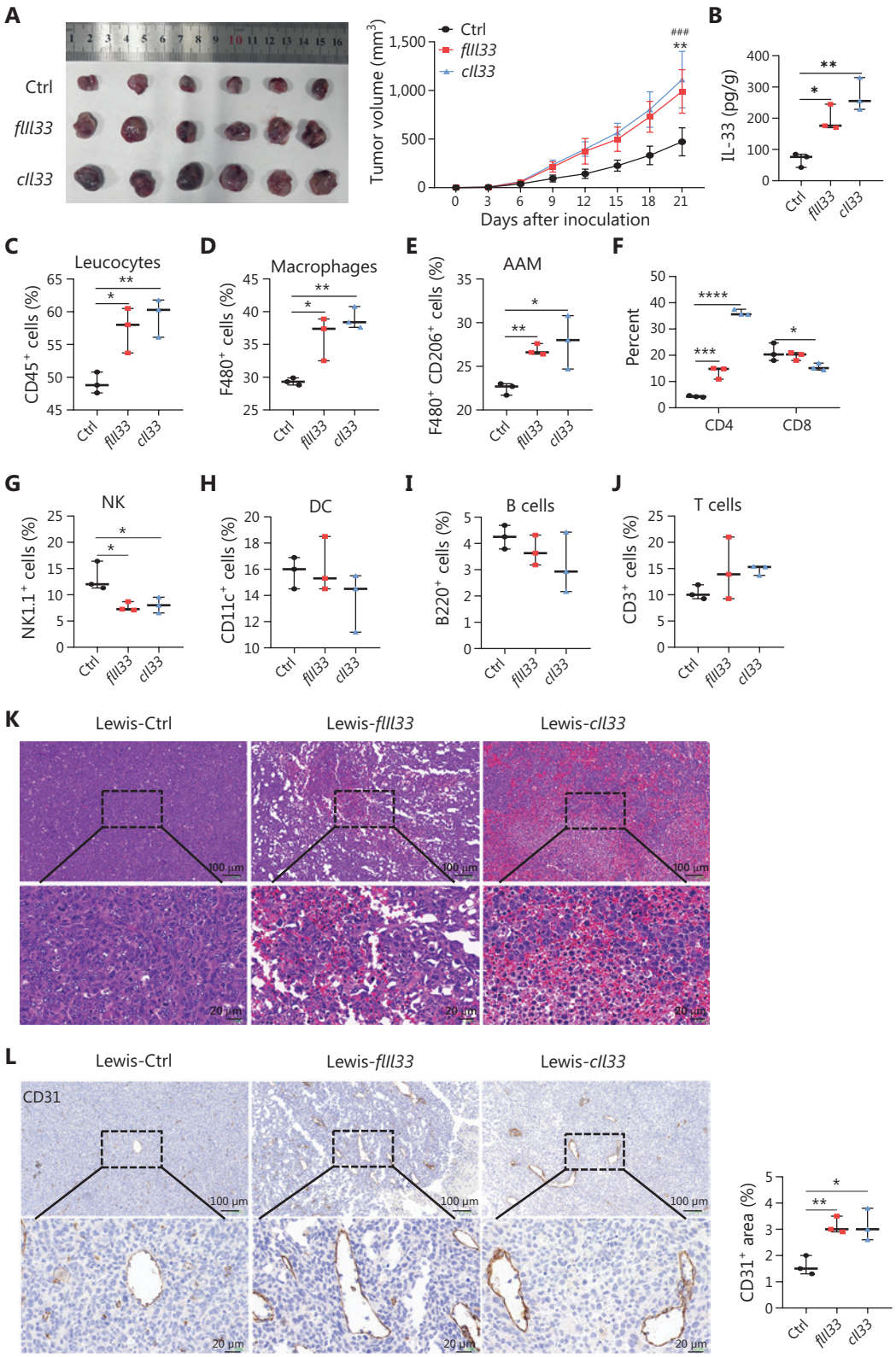


Figure 3 IL-33/ST2 creates an immunosuppressive tumor microenvironment. (A) Tumor size (left) and the change in tumor volume (right) after Lewis-Ctrl (Ctrl), Lewis-*fIl33* (*fIl33*), and Lewis-*cIl33* (*cIl33*) cells were inoculated in WT mice (n = 6), *Lewis-Ctrl *vs.* Lewis-*fIl33*, # Lewis-Ctrl *vs.* Lewis-*cIl33*; (B) Detection of IL-33 in the tumor tissues of Lewis-Ctrl, Lewis-*fIl33*, and Lewis-*cIl33* groups using ELISA; (C-J) The

proportion of immune cells in tumor tissues of Lewis-Ctrl, Lewis-*flIl33*, and Lewis-*cIl33* groups detected by flow cytometry. (C) Proportion of $CD45^+$ cells in live cells; (D) Proportion of $F4/80^+$ cells in $CD45^+$ cells; (E) Proportion of $F4/80^+$ $CD206^+$ cells in $CD45^+$ cells; (F) Percentage of $CD4^+$ and $CD8^+$ T cells in $CD3^+$ cells; (G) Proportion of $NK1.1^+$ cells in $CD45^+$ cells; (H) Proportion of $CD11C^+$ cells in $CD45^+$ cells; (I) Proportion of $B220^+$ cells in $CD45^+$ cells; (J) Proportion of $CD3^+$ cells in $CD45^+$ cells; (K) Representative H&E stained images of tumor tissues from Lewis-Ctrl, Lewis-*flIl33*, and Lewis-*cIl33* groups. Scale bar, 100 μm (up), 20 μm (down); (L) Representative IHC stainedimages (left) and quantification analysis (right) of CD31 in tumor tissues from Lewis-Ctrl, Lewis-*flIl33*, and Lewis-*cIl33* groups. Scale bar, 100 μm (up), 20 μm (down). Data are shown as the mean ± SD and analysed using one-way ANOVA. $^*P < 0.05$, $^{**}P < 0.01$, $^{***}P < 0.001$, $^{****}P < 0.0001$, $^{\#\#\#}P < 0.001$. IL-33, interleukin-33; ST2, suppression of tumorigenicity 2; AAM, alternatively activated macrophages; ELISA, enzyme-linked immunosorbent assay; H&E, haematoxylin and eosin; IHC, immunohistochemistry.

inhibit tumor growth *in vivo*. WT and $St2^{-/-}$ BMDMs were administered *via* tail vein injection into mice with carcinoma *in situ*. The $St2^{-/-}$ BMDM-treated group inhibited tumor growth (**Figure 2C**). Expression of CD31 in tumor tissues was assessed to determine the effect of $St2^{-/-}$ BMDMs on angiogenesis. IHC results showed that $St2^{-/-}$ BMDMs inhibited CD31 expression (**Figure 2D**). Immunofluorescence staining of ST2 and the marker of AAMs (CD206) in mouse tumor tissues showed that the $St2^{-/-}$ BMDM-treated group exhibited fewer $ST2^+$ AAMs than the WT BMDMs group (**Figure 2E**). Thus, transfer of $St2^{-/-}$ BMDMs inhibited tumor growth by decreasing polarization of AAMs in the TME.

IL-33/ST2 creates an immunosuppressive TME

A lentivirus containing *flIl33* and *cIl33* without the nuclear localisation domain was constructed to determine the local effects of the IL-33/ST2 axis on tumor growth and eliminate the potential ST2-independent functions of flIL-33[30]. Lewis cells overexpressing *flIl33* (Lewis-*flIl33*), *cIl33* (Lewis-*cIl33*), and a control (Lewis-Ctrl) were successfully generated. Lewis-Ctrl, Lewis-*flIl33* and Lewis-*cIl33* were implanted intradermally into WT mice to assay the effects of IL-33/ST2 *in vivo*. Tumor growth was significantly promoted in the Lewis-*flIl33* and Lewis-*cIl33* groups compared to the Lewis-Ctrl group (**Figure 3A**). Moreover, the ELISA results showed that IL-33 levels increased in the tumor tissues of the Lewis-*flIl33* and Lewis-*cIl33* groups (**Figure 3B**). The expression profiles of various immune cell populations were assessed using flow cytometry to determine the effect of local IL-33 on the TME. The proportion of leucocytes, macrophages, AAMs, and $CD4^+$ T cells increased in the Lewis-*flIl33* and Lewis-*cIl33* groups, while the proportion of natural killer (NK) cells decreased compared to the Lewis-Ctrl group; the decreased proportion of $CD8^+$ T cells only occurred in Lewis-*cIl33* groups (**Figure 3C-G**, **Figure S2A-E**). No significant changes in other immune cells, such as dendritic cells (DC) cells, T cells, and B cells, were detected (**Figure 3H-J**, **Figure S2F-H**). Immunohistochemistry (IHC) and H&E staining were used to detect pathologic changes in the tumor tissues to further determine the effect of IL-33 on the TME. Severe necrosis and immune cell infiltration were noted in the Lewis-*flIl33* and Lewis-*cIl33* groups compared to the control group (**Figure 3K**). IHC analysis showed increased expression of CD31 in the Lewis-*flIl33* and Lewis-*cIl33* groups (**Figure 3L**). Taken together, these results suggested that IL-33/ST2 exerts a pro-tumor effect by creating an immunosuppressive microenvironment.

IL-33 secreted by tumor cells promotes AAM polarization *via* ST2

IL-33 is known to promote tumor growth by increasing AAM-type macrophage infiltration *via* the ST2 axis in B16 melanoma[23]. Lewis (Lewis-NC), Lewis-Ctrl, Lewis-*flIl33*, and Lewis-*cIl33* cells were co-cultured with WT BMDMs *in vitro* to determine if IL-33 influences lung cancer development by affecting macrophage polarization in the TME. The flow cytometry results showed that AAMs increased in the Lewis-*flIl33* and Lewis-*cIl33* groups (**Figure 4A**, **Figure S3A**). The levels of CD206 protein and *Mrc1*, *Arg1*, and *Tgfb* gene expression were upregulated in WT BMDMs in the Lewis-*flIl33* and Lewis-*cIl33* groups (**Figure 4B, C**). Conditioned media were collected from Lewis-NC, Lewis-Ctrl, Lewis-*flIl33*, and Lewis-*cIl33* cells, which were co-cultured with WT BMDMs, compared to media from cells that were not co-cultured to determine the secretion of IL-33. Lewis-*flIl33* and Lewis-*cIl33* cells secreted IL-33 with greater secretion by Lewis-*cIl33* cells than Lewis-*flIl33* cells. Moreover, Lewis-*flIl33* and Lewis-*cIl33* cells promoted secretion of IL-33 from macrophages (**Figure 4D**). $St2^{-/-}$ BMDMs were co-cultured with Lewis-Ctrl,

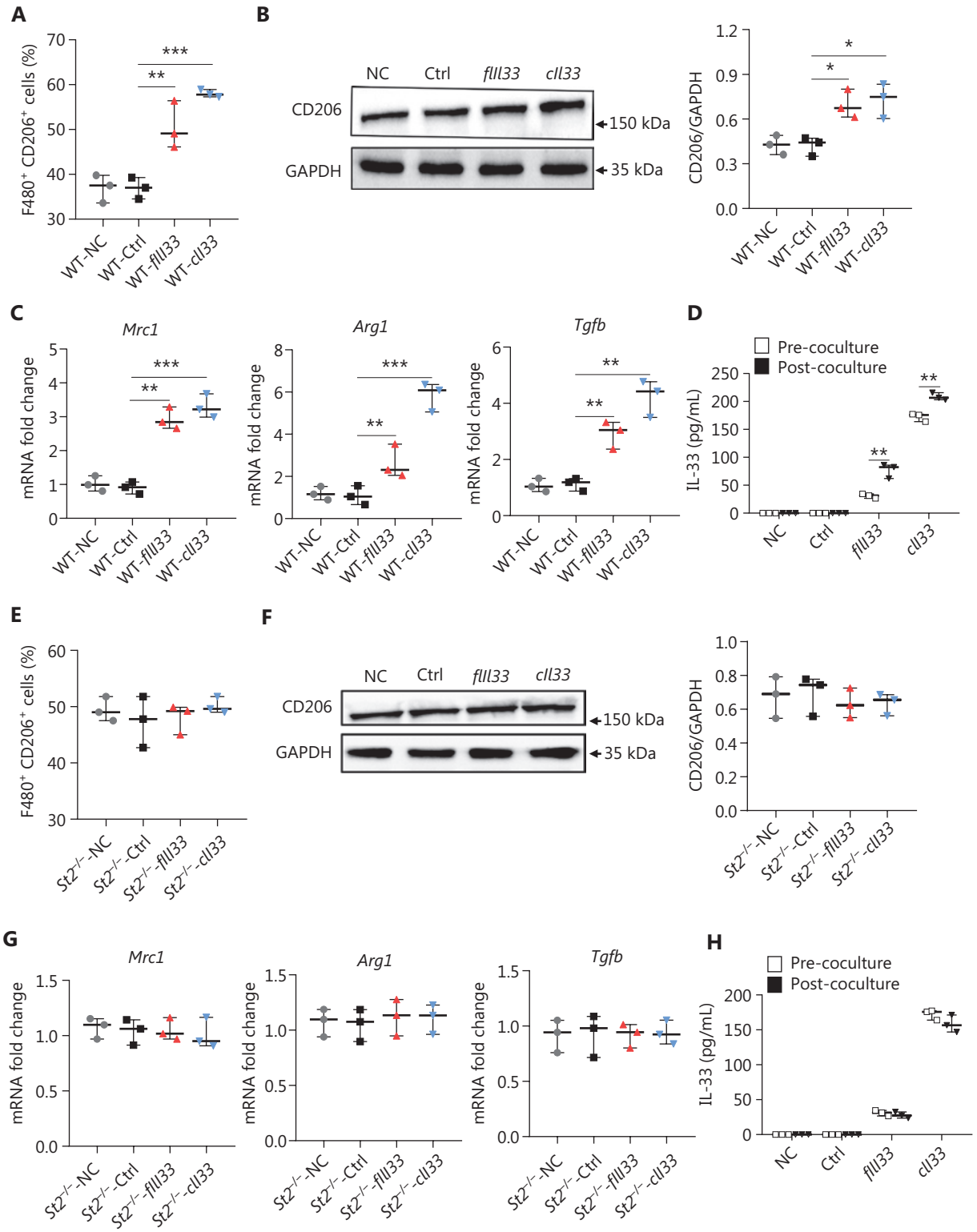


Figure 4 IL-33 secreted by tumor cells promotes AAM polarization. (A-D) WT BMDMs were co-cultured with Lewis-NC (WT-NC), Lewis-Ctrl (WT-Ctrl), Lewis-*fIII33* (WT-*fIII33*), and Lewis-*cII33* cells (WT-*cII33*) for 48 h. (A) The proportion of F4/80$^+$ CD206$^+$ cells of WT BMDMs in co-culture systems detected using flow cytometry; (B) The protein expression of CD206 of WT BMDMs in co-culture systems detected using western blot (left) and quantification was analysed by ImageJ (right); (C) WT BMDM *Mrc1*, *Tgfb*, and *Arg1* mRNA expression in co-culture systems

detected using qPCR; (D) Expression of IL-33 in supernatants of Lewis-NC, Lewis-Ctrl, Lewis-*flIl33*, and Lewis-*cIl33* cells before and after culture with WT BMDMs detected using ELISA; (E-H) $St2^{-/-}$ BMDMs were co-cultured with Lewis-NC ($St2^{-/-}$-NC), Lewis-Ctrl ($St2^{-/-}$-Ctrl), Lewis-*flIl33* ($St2^{-/-}$-*flIl33*), and Lewis-*cIl33* cells ($St2^{-/-}$-*cIl33*) for 48 h. (E) The proportion of F4/80$^+$ CD206$^+$ cells of $St2^{-/-}$ BMDMs in co-culture systems detected using flow cytometry; (F) BMDM CD206 of $St2^{-/-}$ protein expression in co-culture systems detected using western blot (left), and quantification was analysed by ImageJ (right); (G) BMDM *Mrc1*, *Tgfb*, and *Arg1* of $St2^{-/-}$ mRNA expression in co-culture systems detected using qPCR; (H) Expression of IL-33 in supernatants of Lewis-NC, Lewis-Ctrl, Lewis-*flIl33*, and Lewis-*cIl33* cells before and after culture with $St2^{-/-}$ BMDMs detected using ELISA. Data are shown as the mean ± SD and analysed using one-way ANOVA or unpaired two-tailed *t*-test. *P < 0.05, **P < 0.01, ***P < 0.001. IL-33, interleukin-33; ST2, suppression of tumorigenicity 2; AAM, alternatively activated macrophages; BMDM, bone marrow-derived macrophages; qPCR, quantitative real-time polymerase chain reaction.

Lewis-*flIl33*, and Lewis-*cIl33* cells to further investigate whether macrophage polarization in the co-culture system was dependent on tumor cell-derived IL-33. Flow cytometry showed that AAMs did not increase in the Lewis-*flIl33* and Lewis-*cIl33* groups (**Figure 4E, Figure S3B**). Moreover, the levels of CD206 protein and *Mrc1*, *Arg1*, and *Tgfb* gene expression were not significantly altered (**Figure 4F, G**) and IL-33 expression did not increase in the supernatant of the co-culture system (**Figure 4H**). Thus, IL-33 secreted by tumor cells promoted IL-33 secretion by macrophages and promoted polarization of AAMs, which was ST2-dependent.

IL-33/ST2 activates PI3K-Akt during polarization of AAMs

Differentially enriched pathways in WT BMDMs, $Il33^{Tg}$ BMDMs, and $St2^{-/-}$ BMDMs stimulated with IL-4 were screened using transcriptome sequencing to identify the relevant IL-33/ST2 pathways in macrophage polarization. A total of 4756 differentially expressed genes were noted at the transcript level in $St2^{-/-}$ BMDMs compared to WT BMDMs, 2220 differentially expressed genes were noted at the transcript level in $Il33^{Tg}$ BMDMs compared to WT BMDMs, and 4215 differentially expressed genes were noted at the transcript level in $St2^{-/-}$ BMDMs compared to $Il33^{Tg}$ BMDMs (**Figure 5A**). The signalling pathways enriched for differentially expressed genes according to the KEGG database showed that the groups were enriched for the PI3K/Akt signalling pathway (**Figure 5B**). In addition, PI3K/Akt signalling was shown to be highly activated in macrophages compared to other immune cells in lung cancer tissues by analysing single-cell sequencing data from 49 patients with lung cancer (**Figure 5C**)[27]. The levels of PI3K, p-PI3K, Akt, and p-Akt expression in WT BMDMs were measured in the co-culture system using western blot to determine whether the IL-33/ST2 axis promotes polarization of AAMs by activating the PI3K/Akt signalling pathway. Lewis-*flIl33* and Lewis-*cIl33* cells co-cultured with WT BMDMs showed enhanced activation of the PI3K/Akt pathway (**Figure 5D, G**). In contrast, no significant changes were noted in the co-culture system with $St2^{-/-}$ BMDMs (**Figure 5E, H**). A PI3K/Akt inhibitor was added to the co-culture system to further explore whether macrophage polarization was promoted through activation of the PI3K/Akt pathway. The levels of CD206 protein were inhibited in BMDMs co-cultured with Lewis-*flIl33* and Lewis-*cIl33* cells after the addition of a PI3K/Akt inhibitor (**Figure 5F, I**). Flow cytometry results showed that AAMs were decreased in BMDMs co-cultured with Lewis-*flIl33* and Lewis-*cIl33* cells after the addition of a PI3K/Akt inhibitor (**Figure 5J**, **Figure S4**). *Mrc1*, *Arg1*, and *Tgfb* gene expression was inhibited in BMDMs co-cultured with Lewis-*flIl33* and Lewis-*cIl33* cells after addition of a PI3K/Akt inhibitor (**Figure 5K**). Overall, these results indicated that the IL-33/ST2 axis activates the PI3K/Akt signalling pathway during AAM polarization.

Macrophages overexpressing Il33 exerts a protumor effect

Single-cell sequencing of samples was performed from 49 patients with lung cancer to determine IL-33 expression in the TME[27]. Macrophages and fibroblasts were the cells expressing IL-33 in the human TME (**Figure 6A**). Lentiviruses were used to transfer *flIl33* and *cIl33* into the BMDMs and co-cultured them with Lewis cells to determine the effect of macrophages expressing *Il33* on lung cancer *in vivo*. Macrophages overexpressing IL-33 promoted the proliferation and invasive ability of Lewis cells (**Figure 6B, C**). Macrophages overexpressing *flIl33* and *cIl33* were stimulated with IL-4 *in vitro* to further determine whether *Il33*-expressing macrophages

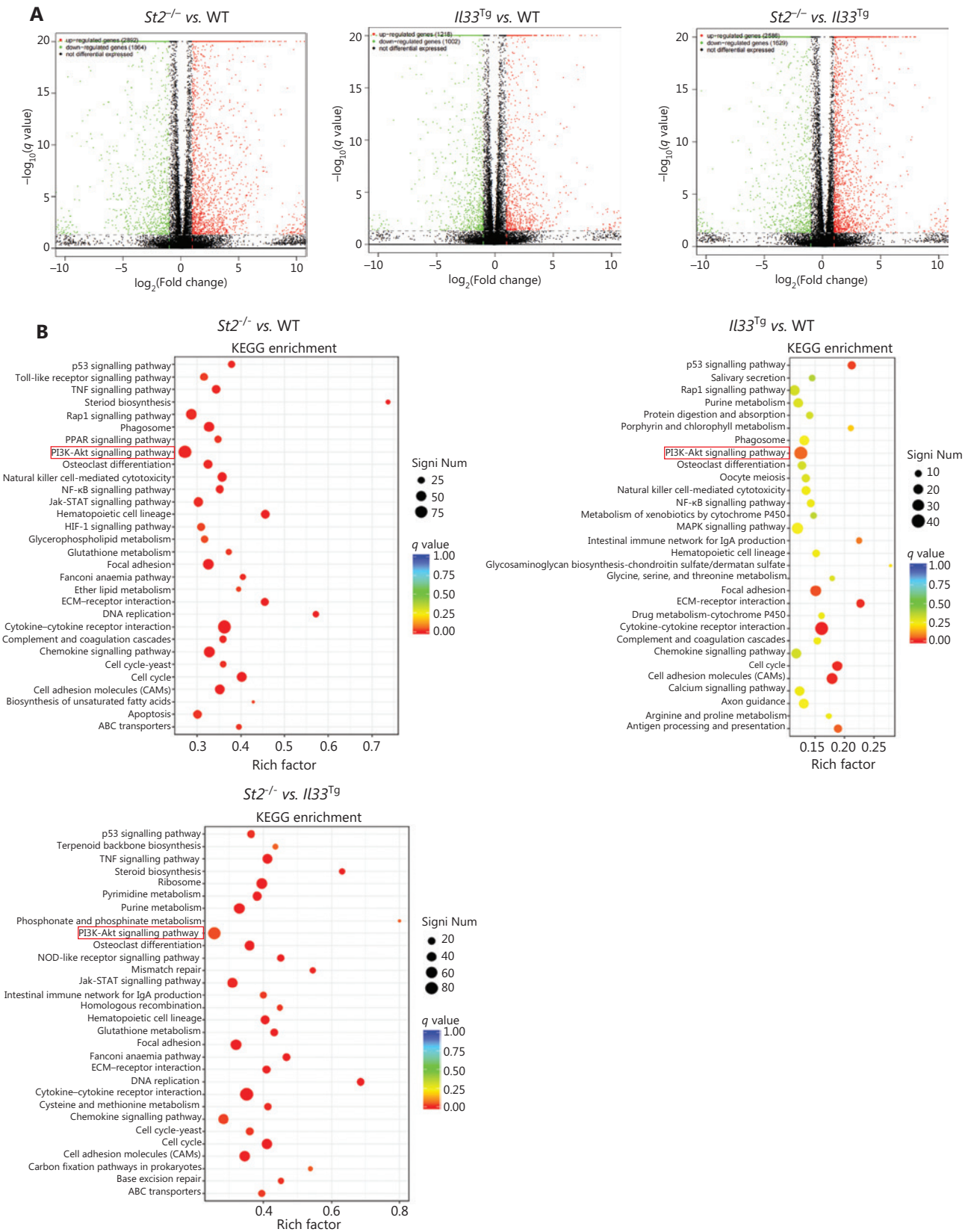


Figure 5 Continued

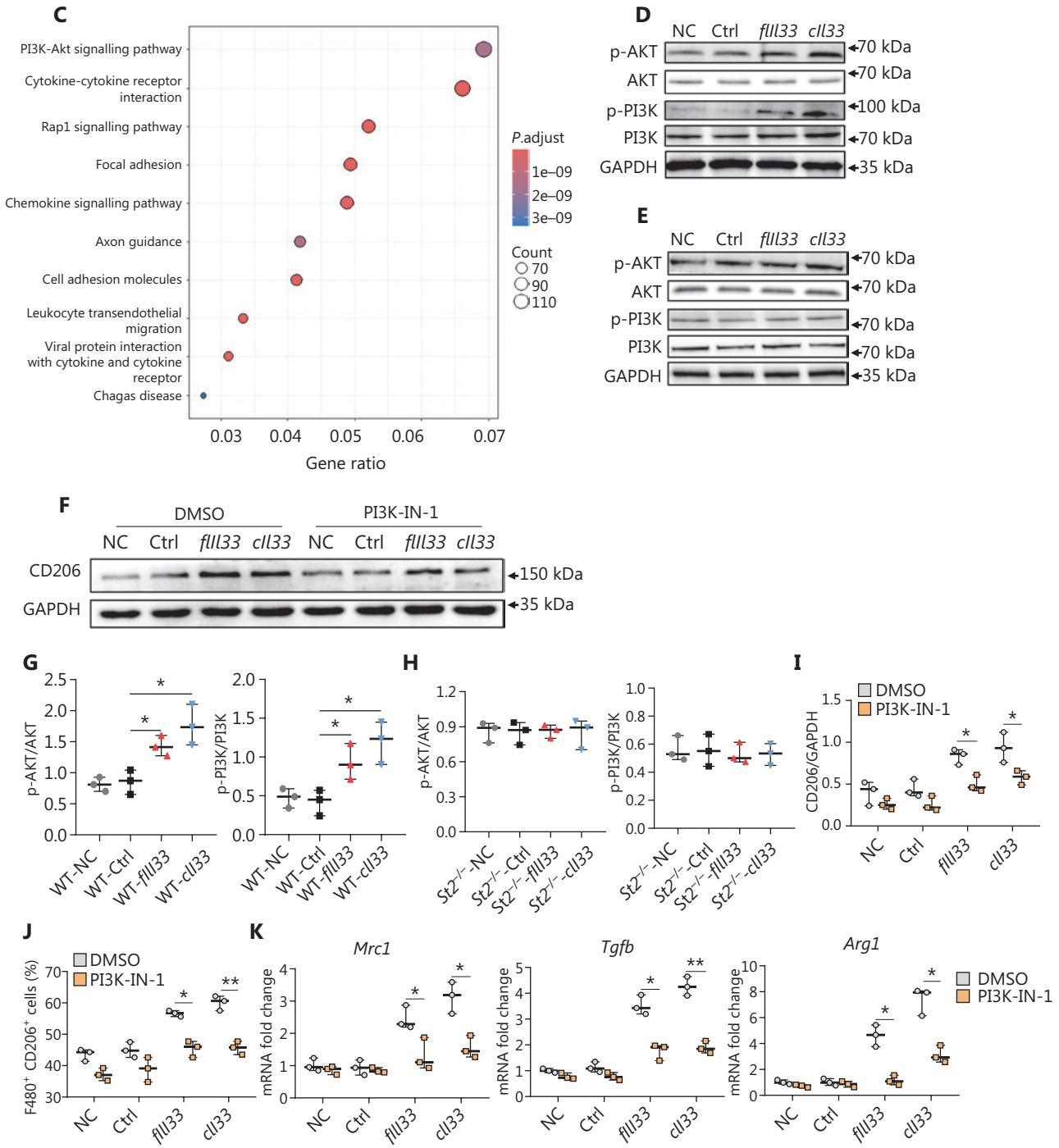


Figure 5 IL-33/ST2 activates PI3K-Akt during polarization of AAMs. (A-B) RNA-seq of IL-4 stimulated BMDMs derived from WT (WT), *St2*$^{-/-}$ (*St2*$^{-/-}$), and *Il33*^{Tg} mice (*Il33*^{Tg}) for 48 h; (A) Volcano plot showing gene distribution of *St2*$^{-/-}$ *vs.* WT, *Il33*^{Tg} *vs.* WT, and *St2*$^{-/-}$ *vs.* *Il33*^{Tg}. Red dots represent upregulation and green dots represent downregulation; (B) Signalling pathways for KEGG enrichment analysis of *St2*$^{-/-}$ *vs.* WT, *Il33*^{Tg} *vs.* WT, and *St2*$^{-/-}$ *vs.* *Il33*^{Tg}; (C) Signalling pathways for KEGG enrichment analysis of macrophages *vs.* other immune cells in lung cancer tissues by analysing single-cell sequencing data from 49 patients with lung cancer; (D) WT BMDM PI3K, p-PI3K, Akt, and p-Akt protein expression co-cultured with Lewis-NC, Lewis-Ctrl, Lewis-*fIll33*, and Lewis-*cIl33* detected using western blot; (E) *St2*$^{-/-}$ BMDM PI3K, p-PI3K, Akt, and p-Akt protein expression co-cultured with Lewis-NC, Lewis-Ctrl, Lewis-*fIll33*, and Lewis-*cIl33* cells detected using western blot; (F) CD206 protein expression derived from WT BMDMs co-cultured with Lewis-NC, Lewis-Ctrl, Lewis-*fIll33*, and Lewis-*cIl33* cells after the addition of a PI3K/Akt

inhibitor was detected using western blot; (G) Quantification of **Figure 5D** was analysed by ImageJ; (H) Quantification of **Figure 5E** was analysed by ImageJ; (I) Quantification of **Figure 5F** was analysed by ImageJ; (J) The proportion of F4/80$^+$ CD206$^+$ cells of WT BMDMs co-cultured with Lewis-NC, Lewis-Ctrl, Lewis-*flIl33*, and Lewis-*cIl33* cells after adding a PI3K/Akt inhibitor detected using flow cytometry; (K) *Mrc1*, *Tgfb*, and *Arg1* mRNA expression in WT BMDMs co-cultured with Lewis-NC, Lewis-Ctrl, Lewis-*flIl33*, and Lewis-*cIl33* cells after adding a PI3K/Akt inhibitor detected using qPCR. Data are shown as the mean ± SD and analysed using an unpaired two-tailed *t*-test. **P* < 0.05, ***P* < 0.01. AAM, alternatively activated macrophages; KEGG, Kyoto Encyclopedia of Genes and Genomes; BMDM, bone marrow-derived macrophages; qPCR, quantitative real-time polymerase chain reaction.

influence macrophage polarization in the TME. The results of flow cytometry suggested that IL-33 promotes IL-4-induced AAM polarization (**Figure 6D**, **Figure S5**). *Mrc1*, *Arg1*, and *Tgfb* gene expression was upregulated in the BMDM-*flIl33* and BMDM-*cIl33* groups compared to the BMDM-Ctrl group (**Figure 6E**). These results indicated that IL-33/ST2 axis-polarized macrophages promote cancer progression.

IL-33/ST2 axis-induced AAMs inhibit the function of T cells by TGF-β

CD4$^+$ and CD8$^+$ T cells were sorted from mouse spleens and cultured in the supernatant derived from BMDMs co-cultured with Lewis-NC, Lewis-Ctrl, Lewis-*flIl33*, and Lewis-*cIl33* cells to further define the role of AAMs in the TME. The ability of CD8$^+$ T cells to secrete IFN-γ and perforin was significantly inhibited by the supernatants from BMDMs co-cultured with Lewis-*flIl33* and Lewis-*cIl33* cells. Furthermore, PD-1 and CTLA4 expression on CD8$^+$ T cells increased when cultured with BMDM supernatants co-cultured with Lewis-*flIl33* and Lewis-*cIl33* cells (**Figure 7A**, **Figure S6A**). Treg differentiation was also promoted in CD4$^+$ T cells cultured with the BMDM supernatants co-cultured with Lewis-*flIl33* and Lewis-*cIl33* cells (**Figure 7B**, **Figure S6B**). The ability of CD4$^+$ T cells to secrete IFN-γ was significantly inhibited when cultured with BMDM supernatants co-cultured with Leiws-*flIl33* and Lewis-*cIl33* cells (**Figure 7C**, **Figure S6C**). ELISA showed that BMDMs co-cultured with Lewis-*flIl33* and Lewis-*cIl33* groups secreted higher TGF-β compared to the Lewis-Ctrl group (**Figure 7D**). TGF-β neutralising antibody was added in the supernatant derived from BMDMs that had been co-cultured with Lewis-*cIl33* cells to confirm that TGF-β influences T cell function. Neutralisation of TGF-β promoted the expression of CD8$^+$ T cell IFN-γ and perforin (**Figure 7E**, **Figure S6D**), inhibited Treg cell differentiation, and promoted CD4$^+$ T cell IFN-γ expression (**Figure 7F**, **Figure S6E**). Taken together, the results demonstrated that the IL-33/ST2 axis promoted secretion of TGF-β from AAMs, which inhibited T cell function.

Discussion

IL-33 exhibits ST2-dependent pro-tumor effects in lung cancer. IL-33 promotes polarization of alternatively activated macrophages by activating the PI3K/Akt signalling pathway[31]. Additionally, IL-33 exhibits an immunosuppressive role by inhibiting T-cell function *via* induction of TGF-β from AAMs[32-34] (**Figure 8**). Furthermore, ST2-deficient macrophages impede tumor growth. Overall, these findings suggest that ST2-expressing macrophages are potential targets for NSCLC immunotherapy.

Patients with NSCLC have enhanced ST2 expression in cancer tissues compared to adjacent healthy tissues and the level of expression correlates with the clinical stage[35]. A previous observational study showed decreased levels of ST2 in lung cancer tissues compared to healthy tissues, which were inversely correlated with cancer stage and survival rates[36]. Our results also showed that higher ST2 expression leads to more aggressive tumor growth. Furthermore, a higher ST2 concentration existed in tumor tissues than adjacent normal tissues in mice. We subsequently extended this finding to the mechanism underlying the role of the IL-33-ST2 axis.

Tumor growth was accelerated in *Il33* transgenic mice, whereas knockout of *Il33* and *St2* inhibited tumor growth. IL-33 is comprised of two distinct functional domains (a nuclear domain that has immunosuppressive functions and an IL-1-like cytokine domain that binds to its receptor ST2)[37-40]. In the current study tumor growth was shown to be significantly promoted in Lewis-*flIl33* and Lewis-*cIl33* mice compared to Lewis-Ctrl mice, highlighting the role of IL-33/ST2 in lung cancer. Collectively, the results suggest that IL-33/ST2 promotes lung cancer progression. Therefore, targeting the IL-33/ST2 axis is a promising immunotherapy for the treatment of NSCLC.

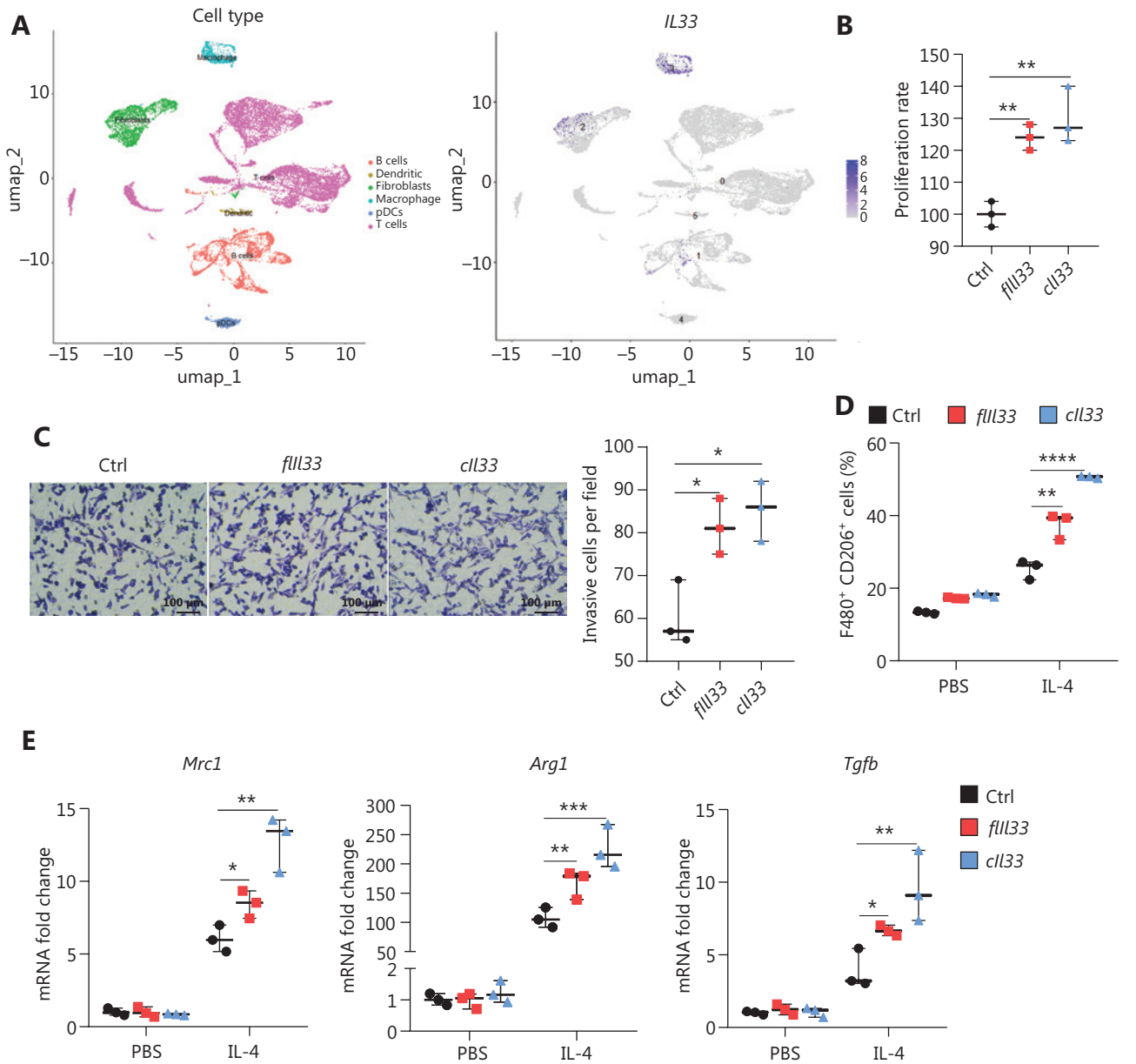


Figure 6 Macrophages overexpressing *Il33* exerts a pro-tumor effect. (A) UMAP demonstrated the distribution and clusters of *Il33* in patients with lung cancer using single-cell RNA-sequencing data; (B) The proliferation of Lewis cells after co-culture with BMDMs-Ctrl (Ctrl), BMDMs-*fIl33* (*fIl33*), and BMDMs-*cIl33* cells (*cIl33*); (C) Invasion of Lewis cells after co-culture with BMDM-Ctrl (Ctrl), BMDM-*fIl33* (*fIl33*), and BMDM-*cIl33* cells (*cIl33*). Scale bar, 100 μm; (D) Expression of AAMs in IL-4 treated BMDM-Ctrl (Ctrl), BMDM-*fIl33* (*fIl33*), and BMDM-*cIl33* cells (*cIl33*) was detected using flow cytometry; (E) *Mrc1*, *Tgfb*, and *Arg1* mRNA expression in IL-4 treated BMDM-Ctrl, BMDM-*fIl33*, and BMDM-*cIl33* cells detected using qPCR. Data are shown as the mean ± SD and were analysed using one-way ANOVA. **P* < 0.05, ***P* < 0.01, ****P* < 0.01, *****P* < 0.0001. UMAP, Uniform Manifold Approximation and Projection; BMDM, bone marrow-derived macrophages; qPCR, quantitative real-time polymerase chain reaction.

Our results showed that IL-33/ST2 can create an immunosuppressive microenvironment by promoting polarization of AAMs, with AAMs serving as recipients and source of IL-33 in the TME, further promoting lung cancer. Notably, Lewis-*fIl33* polarizes macrophages toward AAMs, although the secreted IL-33 level was significantly lower in Lewis-*fIl33* than Lewis-*cIl33*, suggesting that low levels of IL-33 may have a pro-tumorigenic role. Owing to pleiotropic functions, IL-33/

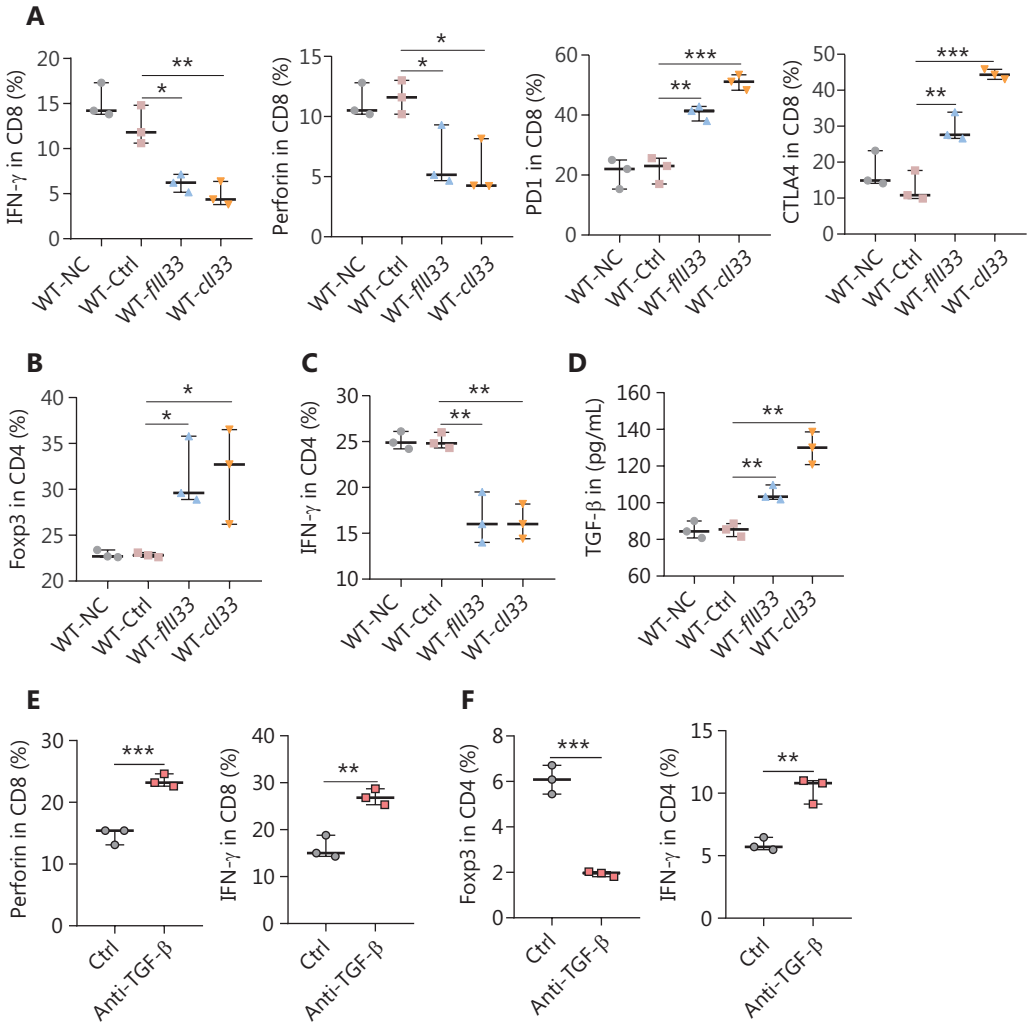


Figure 7 IL-33/ST2 axis-induced AAMs inhibit the function of T cells by TGF-β. (A) The proportion of IFN-γ, perforin, PD1, and CTLA4 in CD8$^+$ T cells cultured with the supernatant from BMDMs that had been co-cultured with Lewis-NC (WT-NC), Lewis-Ctrl (WT-Ctrl), Leiws-*fIl33* (WT-*fIl33*), and Lewis-*cIl33* cells (WT-*cIl33*) detected using flow cytometry; (B) The proportion of Foxp3 in CD4$^+$ T cells cultured with the supernatants from BMDMs that had been co-cultured with Lewis-NC, Lewis-Ctrl, Leiws-*fIl33*, and Lewis-*cIl33* cells was detected by FCS; (C) Proportion of IFN-γ in CD4$^+$ T cells cultured with the supernatant from BMDMs that had been co-cultured with Lewis-NC, Lewis-Ctrl, Leiws-*fIl33*, and Lewis-*cIl33* cells detected using flow cytometry; (D) Level of TGF-β in the supernatant of BMDMs that had been co-cultured with Lewis-NC, Lewis-Ctrl, Leiws-*fIl33*, and Lewis-*cIl33* cells detected using ELISA; (E-G) TGF-β neutralizing antibody was added to the supernatant derived from BMDMs that had been co-cultured with Lewis-*cIl33*, then cultured with T cells; (E) flow cytometry detected the proportion of IFN-γ and perforin in CD8$^+$ T cells; (F) proportion of Foxp3 and IFN-γ in CD4$^+$ T cells detected using flow cytometry. Data are shown as the mean ± SD and analysed using one-way ANOVA and an unpaired two-tailed *t*-test. **P* < 0.05, ***P* < 0.01, ****P* < 0.001. AAM, alternatively activated macrophages; BMDM, bone marrow-derived macrophages; TGF-β, transforming growth factor β; ELISA, enzyme-linked immunosorbent assay.

ST2 modulates recruitment of immune cells and the TME, which exhibit pro- or anti-tumorigenic effects depending on surrounding cellular and soluble factors in the TME[41-43]. Additionally, the IL-33/ST2 axis has been documented to enhance the differentiation and maturation of DC cells, consequently bolstering the anti-tumor efficacy of CD8$^+$ T and NK cells, while concurrently suppressing the proliferation of lung cancer cells[44]. This discrepancy can be attributed to the heterogeneity and complexity of TME components[45].

PI3K/Akt signalling mediated by mTORC1 regulates the effector responses of macrophages, which in turn affect innate immune responses[46] and macrophage polarization[47].

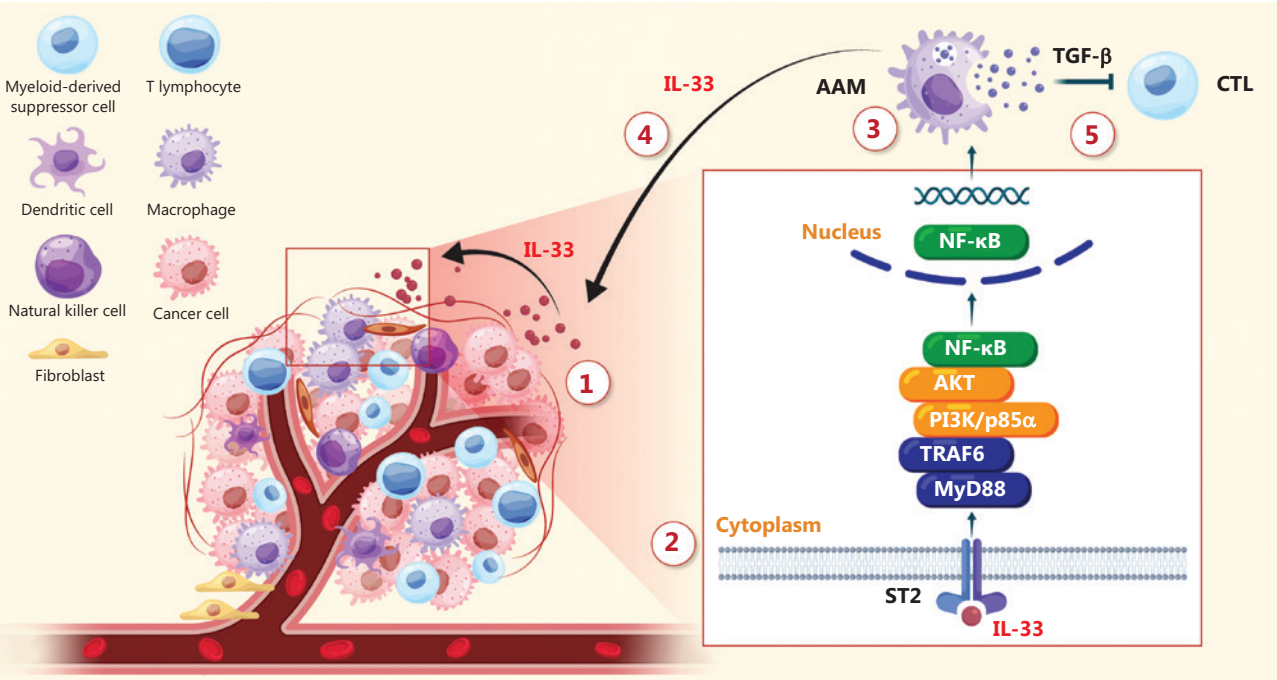


Figure 8 IL-33 fuelling lung cancer *via* alternatively activated macrophage (AAM) polarization. 1) Tumor cell-derived IL-33 binds the ST2 receptor on macrophages; 2) IL-33/ST2 signalling activates the PI3K/AKT pathway through MyD88/TRAF6/NF-κB[31]; 3) Activated macrophages adopt an AAM phenotype; 4) AAMs secrete IL-33[32,33], reinforcing a positive feedback loop; 5) AAMs release TGF-β, suppressing T-cell function and facilitating lung cancer progression[34]. IL-33, interleukin-33; ST2, IL-33 receptor, suppression of tumorigenicity 2; PI3K, phosphoinositide 3-kinase; AKT, protein kinase B; MyD88, myeloid differentiation primary response protein 88; TRAF6, TNF receptor-associated factor 6; NF-κB, nuclear factor-kappa B; TGF-β, transforming growth factor-beta; CTL, cytotoxic T lymphocyte.

In addition, the IL-33/ST2 axis activates the PI3K/AKT/NF-κB signalling pathway through TRAF6, thereby promoting VEGFA-mediated tumor angiogenesis[31]. In the current study IL-33 was shown to induce polarization of AAMs by activating the PI3K/Akt pathway, which is consistent with the findings of a previous study[48].

Direct activation of ST2 *via* stimulation with IL-33 decreases PD-1 expression in CTLs[49]. However, IL-33-polarized AAMs were shown to promote PD1 and CTLA4 expression in $CD8^+$ T cells. Increased infiltration of $CD4^+$ within Lewis-*flIl33* and Lewis-*cIl33* tumors was noted compared to Lewis-Ctrl tumors, but decreased infiltration of $CD8^+$ T cells was only occurred in Lewis-*cIl33* compared to Lewis-Ctrl tumors. In addition, a notably high proportion of $CD3^+CD4^-CD8^-$ cells was detected in these tumors, which is consistent with previous findings[50]. We hypothesise that these cells contribute to the tumor immunosuppressive microenvironment. Moreover, the secretion of TGF-β by IL-33/ST2-polarized AAMs promoted the differentiation of Treg cells and inhibited the secretion of IFN-γ and perforin by $CD8^+$ T cells.

Several major treatment options are available for NSCLC. Lobectomy is currently considered the best treatment for early-stage NSCLC[51,52]. Neoadjuvant chemotherapy is feasible and immunotherapy may be the best therapeutic strategy for neoadjuvant treatment of early-stage NSCLC[53]. The most common immune checkpoint inhibitors, such as PD1, PDL1, and CTLA-4 blockade and CAR-T, have been used to treat NSCLC[54-56]. While anti-monoclonal antibodies have been used in clinical applications, the efficacy in cases of poor prognosis may be compromised by factors, such as dysregulation of cytokine expression, including IL-33. Our results highlight the potential of ST2 as a therapeutic target for NSCLC immunotherapy.

The findings herein support targeting of the pro-tumor cytokine, IL-33, and its receptor (ST2) as an effective strategy to convert the immunoevasive TME into an immunoreactive TME for tumor therapy.

Acknowledgements

We thank Professor 'Eddy' Foo Y. Liew, FRS of the University of Glasgow for his help in designing this project and proof-reading the manuscript.

Grant support

This study was supported by the National Key R&D Program of China (2023YFC2413100), the National Natural Science Foundation of China (No. 81501423), and the Fundamental Research Funds for the Central Universities.

Conflict of interest statement

No potential conflicts of interest are disclosed.

Author contributions

Conceived and designed the analysis: Liping Liu, Dong Li.
Collected the data: Liping Liu, Yingdong Xie, Ying Wang.
Contributed data or analysis tools: Liping Liu, Haoge Luo.
Performed the analysis: Liping Liu, Haoge Luo, Shiying Ren, Haiyang Sun.
Wrote the paper: Liping Liu, Dong Li.

Data availability statement

The raw sequence data reported in this paper have been deposited in the Genome Sequence Archive (Genomics, Proteomics & Bioinformatics 2021) in the National Genomics Data Center (Nucleic Acids Res 2022), China National Center for Bioinformation/Beijing Institute of Genomics, Chinese Academy of Sciences (GSA: CRA021020), which are publicly accessible at https://ngdc.cncb.ac.cn/gsat.

References

1. Siegel RL, Miller KD, Fuchs HE, Jemal A. Cancer statistics, 2021. CA Cancer J Clin. 2021; 71: 7-33.
2. Siegel RL, Miller KD, Jemal A. Cancer statistics, 2017. CA Cancer J Clin. 2017; 67: 7-30.
3. Cook S, Samuel V, Meyers DE, Stukalin I, Litt I, Sangha R, et al. Immune-related adverse events and survival among patients with metastatic NSCLC treated with immune checkpoint inhibitors. JAMA Netw Open. 2024; 7: e2352302.
4. Miller M, Hanna N. Advances in systemic therapy for non-small cell lung cancer. BMJ. 2021; 375: n2363.
5. Chen L, Chen F, Li J, Pu Y, Yang C, Wang Y, et al. CAR-T cell therapy for lung cancer: potential and perspective. Thorac Cancer. 2022; 13: 889-99.
6. Klemm F, Joyce JA. Microenvironmental regulation of therapeutic response in cancer. Trends Cell Biol. 2015; 25: 198-213.
7. Junttila MR, de Sauvage FJ. Influence of tumour micro-environment heterogeneity on therapeutic response. Nature. 2013; 501: 346-54.
8. Xu D, Chan WL, Leung BP, Huang Fp, Wheeler R, Piedrafita D, et al. Selective expression of a stable cell surface molecule on type 2 but not type 1 helper T cells. J Exp Med. 1998; 187: 787-94.
9. Tominaga S. A putative protein of a growth specific cDNA from BALB/c-3T3 cells is highly similar to the extracellular portion of mouse interleukin 1 receptor. FEBS Lett. 1989; 258: 301-4.
10. Hayakawa H, Hayakawa M, Kume A, Tominaga S. Soluble ST2 blocks interleukin-33 signaling in allergic airway inflammation. J Biol Chem. 2007; 282: 26369-80.
11. Chang CP, Hu MH, Hsiao YP, Wang YC. ST2 signaling in the tumor microenvironment. Adv Exp Med Biol. 2020; 1240: 83-93.
12. Zhou Q, Wu X, Wang X, Yu Z, Pan T, Li Z, et al. The reciprocal interaction between tumor cells and activated fibroblasts mediated by TNF-α/IL-33/ST2L signaling promotes gastric cancer metastasis. Oncogene. 2020; 39: 1414-28.
13. Yang Y-E, Hu M-H, Zeng Y-C, Tseng Y-L, Chen Y-Y , Su W-C, et al. IL-33/NF-κB/ST2L/Rab37 positive-feedback loop promotes M2 macrophage to limit chemotherapeutic efficacy in lung cancer. Cell Death Dis. 2024; 15: 356.
14. Jiang W, Lian J, Yue Y, Zhang Y. IL-33/ST2 as a potential target for tumor immunotherapy. Eur J Immunol. 2021; 51: 1943-55.
15. Akimoto M, Susa T, Okudaira N, Koshikawa N, Hisaki H, Iizuka M, et al. Hypoxia induces downregulation of the tumor-suppressive sST2 in colorectal cancer cells via the HIF-nuclear IL-33-GATA3 pathway. Proc Natl Acad Sci U S A. 2023; 120: e2218033120.
16. Tariq M, Zhang J, Liang G, Ding L, He Q, Yang B. Macrophage polarization: anti-cancer strategies to target tumor-associated macrophage in breast cancer. J Cell Biochem. 2017; 118: 2484-501.
17. Solinas G, Schiarea S, Liguori M, Fabbri M, Pesce S, Zammataro L, et al. Tumor-conditioned macrophages secrete migration-stimulating factor: a new marker for M2-polarization, influencing tumor cell motility. J Immunol. 2010; 185: 642-52.
18. Chanmee T, Ontong P, Konno K, Itano N. Tumor-associated macrophages as major players in the tumor microenvironment. Cancers (Basel). 2014; 6: 1670-90.
19. Gao J, Liang Y, Wang L. Shaping polarization of tumor-associated macrophages in cancer immunotherapy. Front Immunol. 2022; 13: 888713.
20. DeNardo DG, Ruffell B. Macrophages as regulators of tumour immunity and immunotherapy. Nat Rev Immunol. 2019; 19: 369-82.
21. Sica A, Mantovani A. Macrophage plasticity and polarization: in vivo veritas. J Clin Invest. 2012; 122: 787-95.

22. Li D, Guabiraba R, Besnard AG, Komai-Koma M, Jabir MS, Zhang L, et al. IL-33 promotes ST2-dependent lung fibrosis by the induction of alternatively activated macrophages and innate lymphoid cells in mice. J Allergy Clin Immunol. 2014; 134: 1422-32.e11.
23. Xu H, Li D, Ma J, Zhao Y, Xu L, Tian R, et al. The IL-33/ST2 axis affects tumor growth by regulating mitophagy in macrophages and reprogramming their polarization. Cancer Biol Med. 2021; 18: 172-83.
24. Cui W, Zhang W, Yuan X, Liu S, Li M, Niu J, et al. Vitamin A deficiency execrates Lewis lung carcinoma via induction of type 2 innate lymphoid cells and alternatively activates macrophages. Food Sci Nutr. 2019; 7: 1288-94.
25. Festing MF, Altman DG. Guidelines for the design and statistical analysis of experiments using laboratory animals. ILAR J. 2002; 43: 244-58.
26. Győrffy B. Transcriptome-level discovery of survival-associated biomarkers and therapy targets in non-small-cell lung cancer. Br J Pharmacol. 2024; 181: 362-74.
27. Maynard A, McCoach CE, Rotow JK, Harris L, Haderk F, Kerr DL, et al. Therapy-induced evolution of human lung cancer revealed by single-cell RNA sequencing. Cell. 2020; 182: 1232-51.e22.
28. Tang Z, Li C, Kang B, Gao G, Li C, Zhang Z. GEPIA: a web server for cancer and normal gene expression profiling and interactive analyses. Nucleic Acids Res. 2017; 45: W98-W102.
29. Komohara Y, Ohnishi K, Kuratsu J, Takeya M. Possible involvement of the M2 anti-inflammatory macrophage phenotype in growth of human gliomas. J Pathol. 2008; 216: 15-24.
30. Dinarello CA. An IL-1 family member requires caspase-1 processing and signals through the ST2 receptor. Immunity. 2005; 23: 461-2.
31. Zhu Y, Lu Y, Zhu Y, Ren X, Deng Q, Yang M, et al. ST2L promotes VEGFA-mediated angiogenesis in gastric cancer by activating TRAF6/PI3K/Akt/NF-κB pathway via IL-33. Sci Rep. 2024; 14: 26393.
32. Liang Y, Yang N, Pan G, Jin B, Wang S, Ji W. Elevated IL-33 promotes expression of MMP2 and MMP9 via activating STAT3 in alveolar macrophages during LPS-induced acute lung injury. Cell Mol Biol Lett. 2018; 23: 52.
33. Zeng F, Chen H, Chen L, Mao J, Cai S, Xiao Y, et al. An autocrine circuit of IL-33 in keratinocytes is involved in the progression of psoriasis. J Invest Dermatol. 2021; 141: 596-606.e7.
34. Mok MY, Luo CY, Huang FP, Kong WY, Chan GCF. IL-33 orchestrated the interaction and immunoregulatory functions of alternatively activated macrophages and regulatory T cells in vitro. J Immunol. 2023; 211: 1134-43.
35. Wang C, Chen Z, Bu X, Han Y, Shan S, Ren T, et al. IL-33 signaling fuels outgrowth and metastasis of human lung cancer. Biochem Biophys Res Commun. 2016; 479: 461-8.
36. Akimoto M, Hayashi JI, Nakae S, Saito H, Takenaga K. Interleukin-33 enhances programmed oncosis of ST2L-positive low-metastatic cells in the tumour microenvironment of lung cancer. Cell Death Dis. 2016; 7: e2057.
37. Cayrol C, Girard JP. IL-33: an alarmin cytokine with crucial roles in innate immunity, inflammation and allergy. Curr Opin Immunol. 2014; 31: 31-7.
38. Millar NL, O'Donnell C, McInnes IB, Brint E. Wounds that heal and wounds that don't – the role of the IL-33/ST2 pathway in tissue repair and tumorigenesis. Semin Cell Dev Biol. 2017; 61: 41-50.
39. Kakkar R, Hei H, Dobner S, Lee RT. Interleukin 33 as a mechanically responsive cytokine secreted by living cells. J Biol Chem. 2012; 287: 6941-8.
40. Lefrançais E, Roga S, Gautier V, Gonzalez-de-Peredo A, Monsarrat B, Girard JP, et al. IL-33 is processed into mature bioactive forms by neutrophil elastase and cathepsin G. Proc Natl Acad Sci U S A. 2012; 109: 1673-8.
41. De la Fuente M, MacDonald TT, Hermoso MA. The IL-33/ST2 axis: role in health and disease. Cytokine Growth Factor Rev. 2015; 26: 615-23.
42. Wang K, Shan S, Yang Z, Gu X, Wang Y, Wang C, et al. IL-33 blockade suppresses tumor growth of human lung cancer through direct and indirect pathways in a preclinical model. Oncotarget. 2017; 8: 68571-82.
43. Xiao P, Wan X, Cui B, Liu Y, Qiu C, Rong J, et al. Interleukin 33 in tumor microenvironment is crucial for the accumulation and function of myeloid-derived suppressor cells. Oncoimmunology. 2016; 5: e1063772.
44. Xu L, Zheng Y, Wang J, Xu Y, Xie Y, Yang ZP. IL33 activates CD8+T and NK cells through MyD88 pathway to suppress the lung cancer cell growth in mice. Biotechnol Lett. 2020; 42: 1113-21.
45. Galon J, Bruni D. Approaches to treat immune hot, altered and cold tumours with combination immunotherapies. Nat Rev Drug Discov. 2019; 18: 197-218.
46. Dibble CC, Cantley LC. Regulation of mTORC1 by PI3K signaling. Trends Cell Biol. 2015; 25: 545-55.
47. Weichhart T, Hengstschläger M, Linke M. Regulation of innate immune cell function by mTOR. Nat Rev Immunol. 2015; 15: 599-614.
48. Wang Z, Wu L, Pan B, Chen Y, Zhang T, Tang N. Interleukin 33 mediates hepatocyte autophagy and innate immune response in the early phase of acetaminophen-induced acute liver injury. Toxicology. 2021; 456: 152788.
49. Liang Y, Wang X, Wang H, Yang W, Yi P, Soong L, et al. IL-33 activates mTORC1 and modulates glycolytic metabolism in $CD8^+$ T cells. Immunology. 2022; 165: 61-73.
50. Prins RM, Incardona F, Lau R, Lee P, Claus S, Zhang W, et al. Characterization of defective CD4-CD8- T cells in murine tumors generated independent of antigen specificity. J Immunol. 2004; 172: 1602-11.
51. Khullar OV, Liu Y, Gillespie T, Higgins KA, Ramalingam S, Lipscomb J, et al. Survival after sublobar resection versus lobectomy for clinical stage IA lung cancer: an analysis from the national cancer data base. J Thorac Oncol. 2015; 10: 1625-33.
52. Billmeier SE, Ayanian JZ, Zaslavsky AM, Nerenz DR, Jaklitsch MT, Rogers SO. Predictors and outcomes of limited resection for

early-stage non-small cell lung cancer. J Natl Cancer Inst. 2011; 103: 1621-9.
53. Kang J, Zhang C, Zhong WZ. Neoadjuvant immunotherapy for non-small cell lung cancer: state of the art. Cancer Commun (Lond). 2021; 41: 287-302.
54. Mamdani H, Matosevic S, Khalid AB, Durm G, Jalal SI. Immunotherapy in lung cancer: current landscape and future directions. Front Immunol. 2022; 13: 823618.
55. Peggs KS, Quezada SA, Chambers CA, Korman AJ, Allison JP. Blockade of CTLA-4 on both effector and regulatory T cell compartments contributes to the antitumor activity of anti-CTLA-4 antibodies. J Exp Med. 2009; 206: 1717-25.
56. Rizvi NA, Mazières J, Planchard D, Stinchcombe TE, Dy GK, Antonia SJ, et al. Activity and safety of nivolumab, an anti-PD-1 immune checkpoint inhibitor, for patients with advanced, refractory squamous non-small-cell lung cancer (CheckMate 063): a phase 2, single-arm trial. Lancet Oncol. 2015; 16: 257-65.

Cite this article as: Liu L, Luo H, Xie Y, Wang Y, Ren S, Sun H, et al. IL-33/ST2 signalling promotes tumor growth by regulating polarization of alternatively activated macrophages. Cancer Biol Med. 2025; 22: 376-395. doi: 10.20892/j.issn.2095-3941.2024.0483